

# A CFD APPROACH TO SPACER GRID OPTIMIZATION FOR IMPROVED DRYOUT PERFORMANCE IN BWR FUEL BUNDLE

T. Strömgren, A. Zhezherun, Y. Le Moigne, J.-M. Le Corre, D.Y. Sheng and S. Perzon

Westinghouse Electric Sweden AB

72163 Västerås, Sweden

[stromgts@westinghouse.com](mailto:stromgts@westinghouse.com); [lecorrjm@westinghouse.com](mailto:lecorrjm@westinghouse.com)

## ABSTRACT

Spacer grids play an important role to ensure high thermal performance of LWR fuel bundles. Modern grids include complex features, such as mixing vanes, which ensure that the coolant enthalpy is properly distributed, avoiding the creation of hot spot and early boiling transition. In the case of BWR fuel bundle, where annular two-phase flow is dominant in the upper part of the bundle, mixing vanes need to be optimized (in term of shape, size, position, orientation, etc) to increase the liquid film flow on the fuel rods, hence enhancing the dryout power.

For a given BWR fuel lattice, the enhancement of dryout power can be achieved by 1) enhancing the drop deposition to the rods, 2) decreasing the drop entrainment from the rods and 3) preventing the liquid to accumulate on the cold walls (bundle box and water channels). In the past, this optimization was performed mainly by investigating the effect of several fuel features with expensive dryout scoping tests. However, the current advances in numerical simulation of two-phase flow in complex geometries allow the use of CFD simulations to perform early and comprehensive grid spacer optimization. This results in a more knowledge-driven optimization work leading to larger dryout power margin while reducing the amount of scoping dryout tests.

In order to perform an efficient and relevant investigation, the selected CFD models are based on an approach where the annular two-phase flow is simplified to focus only on the parameters of interest. A CFD model with Lagrangian particle tracking is used in order to simulate the flow and droplet deposition in an adiabatic BWR fuel bundle, over a grid span. In order to study how droplet size affects the deposition, a range of different particle Stokes numbers is considered.

The current aim of the CFD calculations is to increase the understanding of how the spacer grid affects the droplet deposition. In the future, CFD simulations can also be used to develop new models to complement three-field subchannel analysis for realistic critical power simulations.

## KEYWORDS

CFD, spacer, mixing vanes, BWR fuel, droplet deposition

## 1. INTRODUCTION

In the design optimization of LWR fuel bundles, spacer grids play an important role to ensure high thermal performance. Spacer grids are typically placed 0.4 to 0.5 m apart along the axial length and have for primary purpose the mechanical integrity of the fuel bundle. However, modern grids include complex features, such as mixing vanes, which ensure that the coolant enthalpy is properly distributed throughout the bundle, avoiding the creation of hot spot and early boiling transition.

## 1.1. BWR Grid Design Optimization

In the case of BWR fuel bundle, where annular two-phase flow is dominant, the boiling transition corresponds to a complete liquid film dryout. The liquid film on the fuel rods is subject to mass exchange by evaporation, drop deposition and drop entrainment. For a given BWR fuel lattice, the enhancement of dryout power can hence be achieved by 1) enhancing the drop deposition to the rods, 2) decreasing the drop entrainment from the rods and 3) preventing the liquid to accumulate on the cold walls (bundle box and water channels). In the past, this optimization was performed mainly by investigating the effect of several fuel features with expensive dryout scoping tests. However, the current advances in numerical simulation of two-phase flow in complex geometries allow the use of CFD simulations to perform early and comprehensive grid spacer optimization. This results in a more knowledge-driven optimization work, potentially leading to better optimized fuel bundle design (e.g. with larger dryout power capability) while reducing the amount of scoping dryout tests.

The mixing vanes have a significant effect on the droplet deposition and hence on the dryout power. Experimentally, up to 15-20% increase in dryout power can be measured. This is achieved by locally increasing the turbulence intensity downstream the grids, by directing the drop flow toward the heated rods and by ripping off the liquid film from cold surfaces. However, the dominant mechanisms and important design parameters to achieve such effects are not well known, considering the complexity of BWR fuel geometry and possible range of operating conditions. Under appropriate assumptions and simplifications, it is proposed to use CFD tools for such investigation with the goal to optimize BWR spacer grids and mixing vanes (in term of shape, size, position, orientation, etc) for increased dryout performance.

## 1.2. Simplified CFD Approach

Multiphase flow is very complex and inherits a broad range of scales and physics which makes it very difficult to simulate, in particular since the applicability of the models are often very parameter dependent. When focusing on BWR spacer grid optimization, one of the main physical phenomena to simulate is the droplet deposition onto the liquid film downstream spacer grids. A simplified approach is hence suggested where a fuel bundle geometry is considered over a single grid span under adiabatic conditions. Further, annular two-phase flow is simulated considering only the steam and drop fields. Drop deposition is modeled using absorbing boundary conditions and no liquid film is considered.

This simplified approach extend the simplified model used in [1] to realistic fuel bundle geometry. Droplet deposition downstream two types of mixing vanes in a single subchannel region (delimited by 4 rods) for several droplet diameters was studied in [1] with CFD simulations using a two-equation  $k-\epsilon$  model for the flow and Lagrangian particle tracking for the droplets. Sensitivity analysis on droplet size and total flowrate were performed. Finally, the enhanced droplet depositions simulated by this approach were input to a 1-D annular-two phase three-field model. Good agreement was found with the experimental information.

A CFD model including both droplet entrainment and deposition was developed in [2]. The simulation results were validated against experimental data. However, the liquid film model could only be used for qualitative and not quantitative studies.

Several studies have also been done on bubbly flow and spacer grids for PWR applications. For instance, the void distribution in a fuel rod bundle with spacer grids using an Euler-Euler model (Two-fluid model) was investigated in [3] in bubbly flow. The simulations were validated against experiments.

### 1.3. Objectives

The aim of this work is to model a BWR fuel bundle geometry (of Westinghouse design) over a grid span, including a spacer grid and surrounded by the fuel channel walls. Drop deposition downstream a BWR spacer is investigated using an Eulerian-Lagrangian CFD model for a range of droplet diameters. This allows to quantify the amount of droplets deposited on each rod, to investigate parameter sensitivities and to investigate how the different mixing vanes in the spacer grid interact with each other. Previously, only a small part of the spacer grid has been modeled when studying droplet deposition using CFD [1].

## 2. MODEL DESCRIPTION

### 2.1. Geometry and Numerical Models

In Figure 1, an outline of the considered geometry is shown. The height of the model is 0.8 m and the spacer grid is placed in the middle. A full Westinghouse SVEA-96 Optima3 quarter bundle geometry is modeled in order to correctly capture the cross flows in the model, i.e. no periodic or symmetry boundary conditions are used. The outer boundary in the model is the fuel channel (and water cross) walls. The rod bundle geometry seen from above with numbered fuel rods is shown in Figure 2. Rods 1, 20 and 24 are not modeled since these rods are part-length rods and the modeled fuel bundle region is located above them.

The distance from the inlet to the spacer grid is 0.4 m and corresponds to about 32 sub-channel hydraulic diameters. This allows the flow to become fully developed before reaching the grid. The distance between the spacer grid and the outlet is also 0.4 m, typical of a BWR grid span.

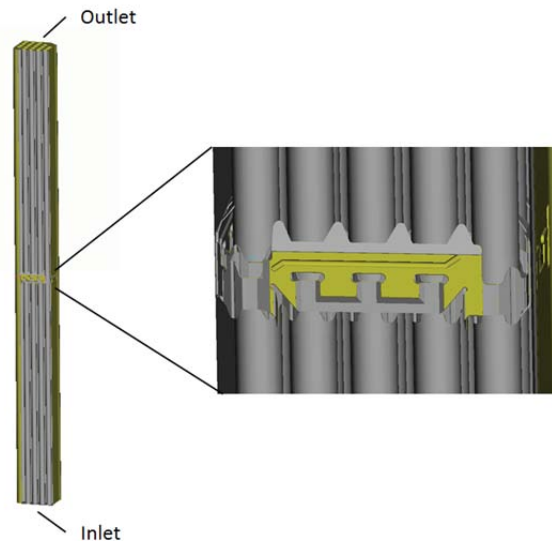


**Figure 1. Outline of model geometry**

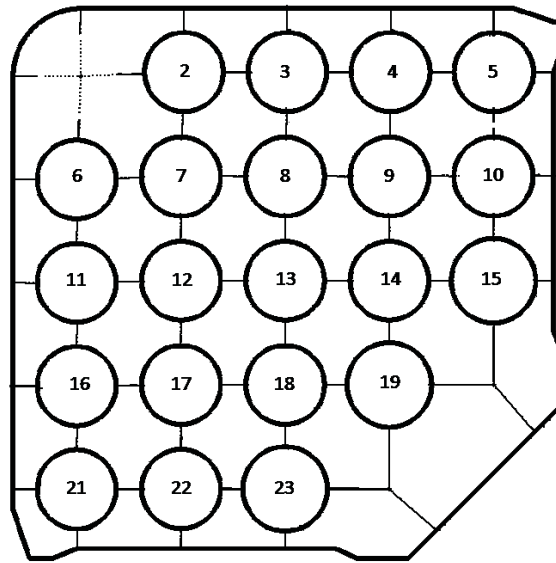


**Figure 2. SVEA-96 Optima3 fuel bundle geometry, numbered rods seen from above**

A Reynolds Averaged Navier Stokes (RANS) model is used to model the flow through the fuel bundle. Steam at 70 bar is used as the continuous fluid (Eulerian phase). The two-equation Realizable k- $\epsilon$  turbulence model is used. Lagrangian particle tracking is used to simulate the droplet transport in the model. The droplets are treated as spherical particles in the model, i.e. the particle diameter is constant and the droplets do not coalesce. Particles are only affected by the drag force (Schiller-Naumann). One-way coupling is assumed – the flow is undisturbed by the droplets and no particle-particle interaction is taken into account. The CFD solver STAR-CCM+ v. 10.02.010 is used.

## 2.2. Boundary Conditions

At the inlet a constant steam velocity is specified and at the outlet a pressure boundary condition is applied. The steam has a no-slip boundary condition on all walls. The particles are injected at the inlet with the same velocity as the steam flow. An escape boundary condition is used at the fuel channel walls and the fuel rods, i.e. droplets that deposit on the boundaries are removed from the model. This is similar to a realistic situation when droplets that deposit form a water film on the surfaces. On the spacer grid and the mixing vanes a rebound boundary condition for the droplets is used with a restitution coefficient set to zero in the normal direction and one in the tangential direction, i.e. droplets hitting the grid or a mixing vane will slide along its surface [2]. This boundary condition is a simplified way of simulating the buildup of a liquid film and the shear off of the liquid film at the edge of the spacer grid, without considering a film model.

## 2.3. Mesh

The mesh is an unstructured polyhedral mesh. The average cell size in the core flow is 0.5 mm. Prism layers are placed on all fuel rods, channel walls and the spacer. The first cell has a  $y^+$  value of around 40 along the fuel rods. The total number of cells is 48.4 million. In Figure 3 the mesh between the fuel rods is shown.

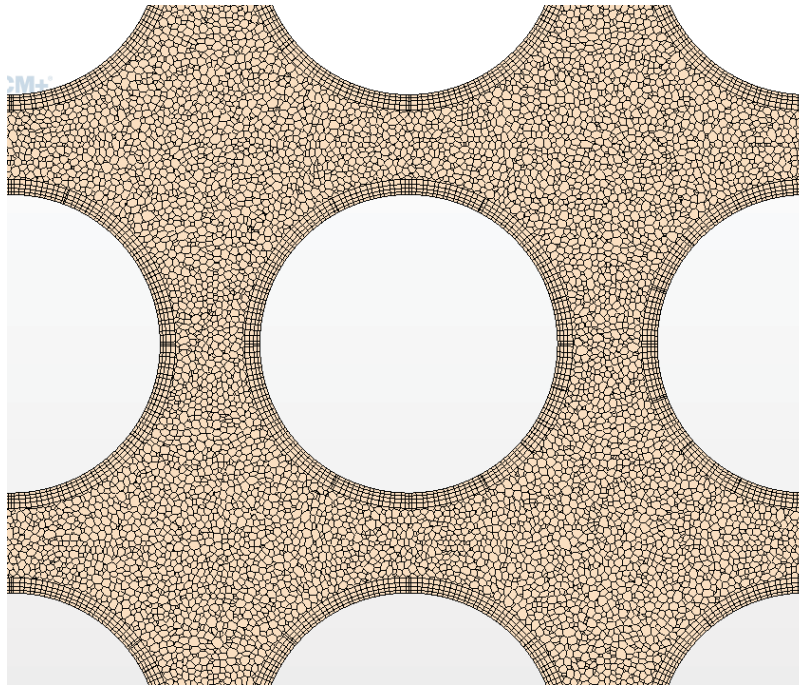


**Figure 3. Mesh around a fuel rod**

## **2.4. Turbulence Models**

The Reynolds stress model was compared to the two-equation  $k-\varepsilon$  model for a 2x2 PWR rod bundle with a simple spacer grid [4]. The Reynolds stress model did reproduce the results earlier obtained with standard two-equation models, however, in strong swirling flow, i.e. downstream the vanes, the Reynolds stress model could improve the simulation results, although at a slightly higher computational cost.

The effect of different turbulence models simulating two subchannels in a PWR is investigated in [5] and show that the SST- $k\omega$  gives a better prediction of the turbulence intensity compared to Realizable  $k-\varepsilon$  model and a Reynolds Stress Model.

In this work the simplest model, the two-equation Realizable  $k-\varepsilon$  turbulence model, is used. Although this model does not capture the anisotropic flows as well as the Reynolds Stress Models, this model is used as a reference point and is considered sufficient to support the comparative study performed in the present work [2].

## **2.5. Simulations**

The inlet velocity and droplet diameter were varied in the simulations. Four different droplet diameters were investigated; 50  $\mu\text{m}$ , 100  $\mu\text{m}$ , 200  $\mu\text{m}$  and 300  $\mu\text{m}$ . A particle flow rate of  $3 \cdot 10^6$  particles per second was used for all cases. The general input data to the CFD model are listed in Table I.

**Table I. Input data for CFD simulations**

Reference pressure [MPa]	7.0
Density of steam [kg/m <sup>3</sup> ]	36.5
Density of droplets [kg/m <sup>3</sup> ]	739.7
Viscosity of steam [Pa s]	1.9·10 <sup>-5</sup>

A length of 16 subchannel diameters immediately downstream the model inlet is removed from the results presented below because of entrance effects affecting the predicted droplet deposition. The same behavior at the inlet is reported for all considered particle diameters.

## 2.6. Limitations

This proposed model has limitations mainly due to the simplifications that were applied (Section 1.2). The simulations are isothermal hence no effects due to film evaporation or induced diversion cross-flow are accounted for. The water films on the rods or the fuel channel walls are not modelled in this study, hence the effect of spacer grids on film entrainment was not considered. A single droplet size is assumed, while a realistic simulation should consider a distribution of droplet diameters. Finally, droplet-droplet interactions are neglected in this simulation although it was reported to have an effect for volume fractions as low of 0.001 [6].

## 3. RESULTS

As mentioned in Section 2.5, simulations were performed using four different particle diameters,  $D_p$ , 50, 100, 200 and 300  $\mu\text{m}$ . The behavior of a particle can be characterized by the Stokes number,  $St$ , defined as [7]

$$St = \tau_p / \tau_g \quad (1)$$

Where  $\tau_g$  is a characteristic time scale of the flow and is defined as  $D_H/U$  where  $D_H$  is the hydraulic diameter of a subchannel and  $U$  is the mean velocity.  $\tau_p$  is the particle response, i.e. the time it takes for a particle to reach 63 % of the free stream velocity; it is generally expressed as:

$$\tau_p = \frac{\rho_p D_p^2}{18\mu_g} \quad (2)$$

where  $\rho_p$ ,  $D_p$  and  $\mu_g$  are the droplet density, droplet diameter and steam dynamic viscosity, respectively. A small Stokes number ( $St \ll 1$ ) corresponds to particles that instantaneously adjust themselves to the flow field and will behave as a passive scalar. Particles with  $St \sim 1$  do not respond to the smaller time scales of the flow while they do respond to larger time scales. For  $St \gg 1$  the particle response time is very large compared to the response time of the flow. Stokes numbers corresponding to the different droplet diameters used in the simulations range from 7 to 246, as shown in Table II.

**Table II. Droplet diameters with corresponding Stokes numbers**

$D_p$ [ $\mu\text{m}$ ]	50	100	200	300
$St$ [-]	7	27	109	246

### 3.1. Droplet Deposition for Different Droplet Diameters

The cumulative deposited droplet mass normalized with the fuel rod with the largest cumulative deposited droplet deposition is shown in Figure 5 for the four different droplet diameters and for six different fuel rods (all located in the center of the considered fuel bundle in Figure 2). The lower part of the spacer grid is placed at height 0 and the extension of the grid is highlighted with red dotted lines. The position of the rods within the bundle can be seen in Figure 2. The large effect of the grid on the enhancement of droplet deposition is clearly visible and is most dominant immediately downstream the grid. It is seen that the smallest cumulative droplet deposition is found for the smallest Stokes number, i.e.  $D_p=50\ \mu\text{m}$ , for all fuel rods in Figure 5 except 13 and 14 where  $D_p=100\ \mu\text{m}$  has the smallest cumulative droplet deposition. The largest cumulative droplet deposition is found for the larger droplet sizes, most commonly for  $D_p=300\ \mu\text{m}$  which is the largest considered Stokes number. An interpretation of these results is that the smaller droplets respond faster to the smaller time scales of the fluid and adjust their trajectories to the flow while the droplets with larger Stokes numbers do not adjust their trajectories to small eddies and therefore have a larger probability to deposit on the walls of the fuel rods.

A qualitative overview of the droplet deposition where the effect of the grid on the deposition is visible is shown in Figure 4. The periphery rods are removed on the side in order to see the droplet deposition on the central rods.

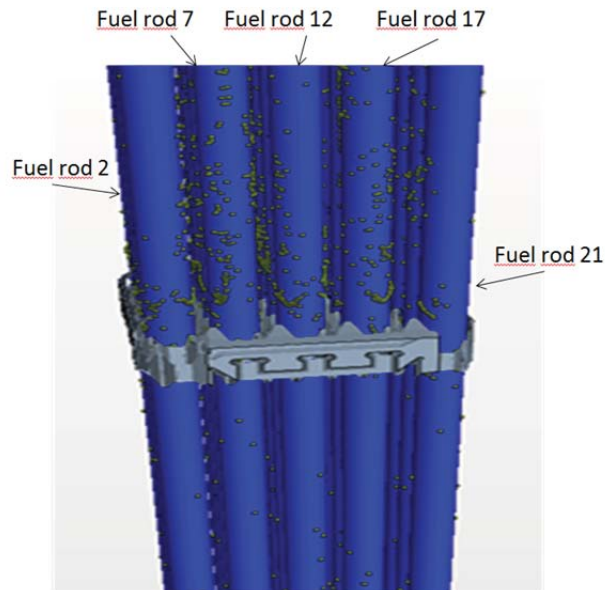


Figure 4. Particle deposition shown for full grid with  $D_p=200\ \mu\text{m}$

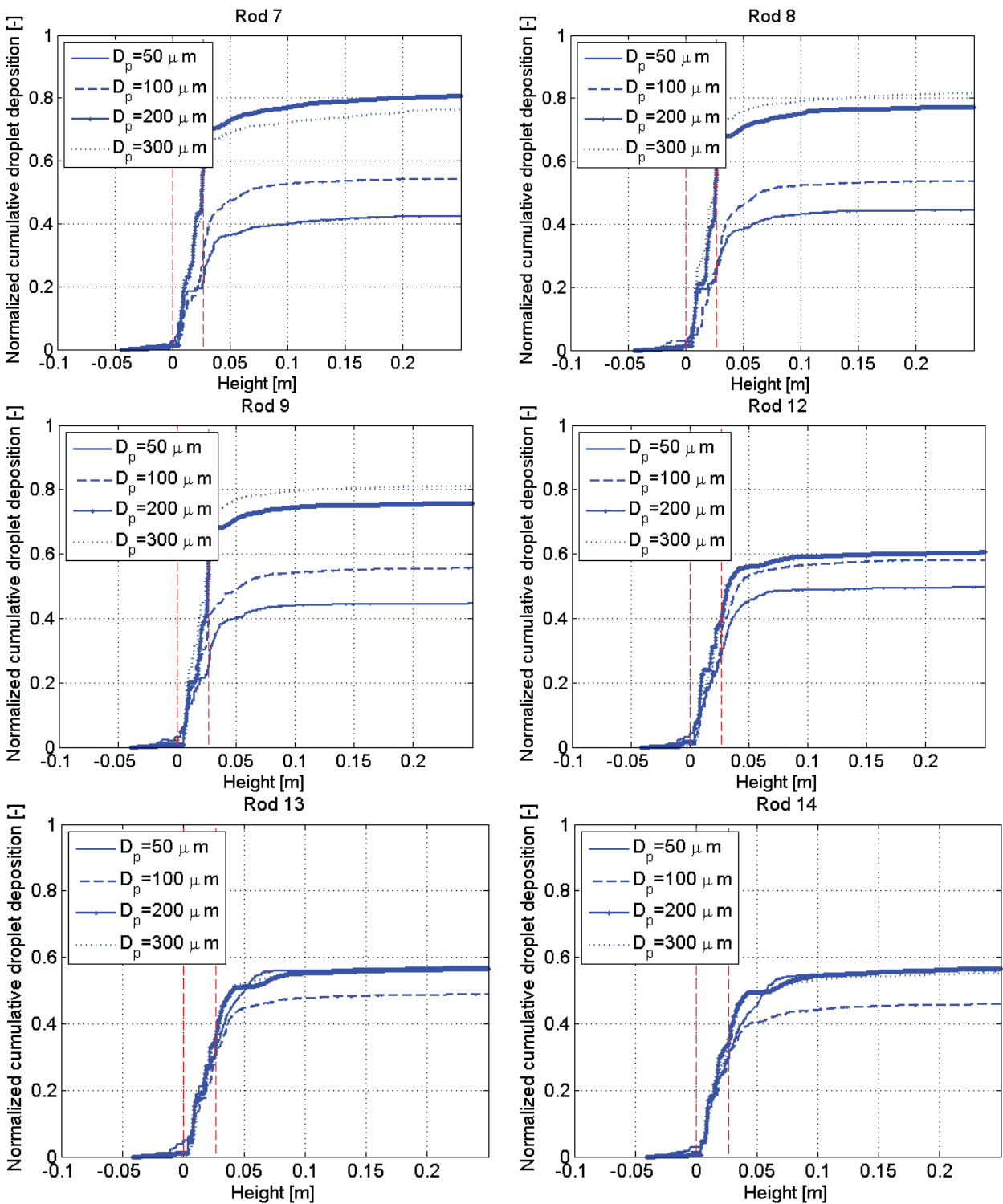


Figure 5. Normalized cumulative droplet deposition for six central rods

### 3.2. Asymmetric Droplet Deposition in Subchannels

It was observed that the droplet deposition within a subchannel (a channel delimited by four rods) was asymmetric between the four  $\frac{1}{4}$ -rods defining the subchannel. A lower droplet deposition was generally found at the fuel rod wall closest to the bottom part of the mixing vane. An enhanced droplet deposition at the fuel rod walls on the side of the mixing vane for spacers with asymmetric shape was observed, both in experiments and simulations, by [2]. The same results have been obtained in the present study.

Figure 6 shows iso plots of the helicity, i.e. the scalar product between the velocity and the vorticity. It is seen that the helicity is not centered in the middle of the subchannels which explains the asymmetry in droplet deposition between the different fuel rods adjacent to a subchannel. This asymmetry lasts all the way to the outlet of the model. The helicity in a cross-section 0.06 m above the spacer is shown in Figure 7, the negative and positive values show different rotational direction of the swirl.

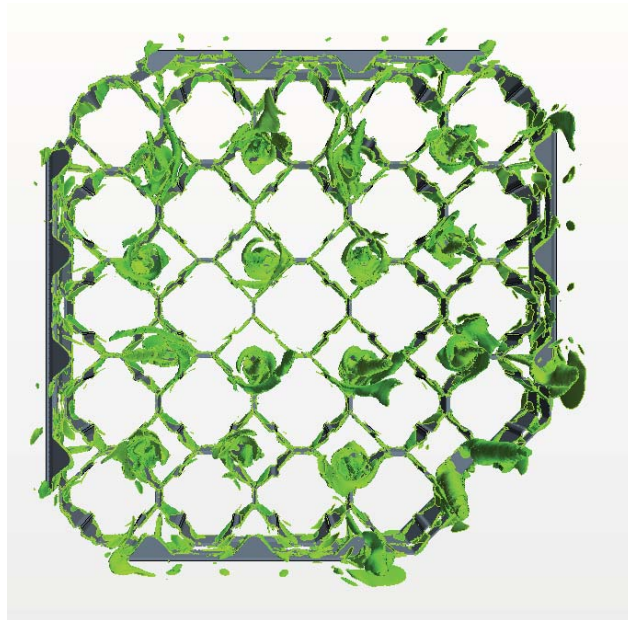


Figure 6. Iso surface of the helicity shown together with the grid

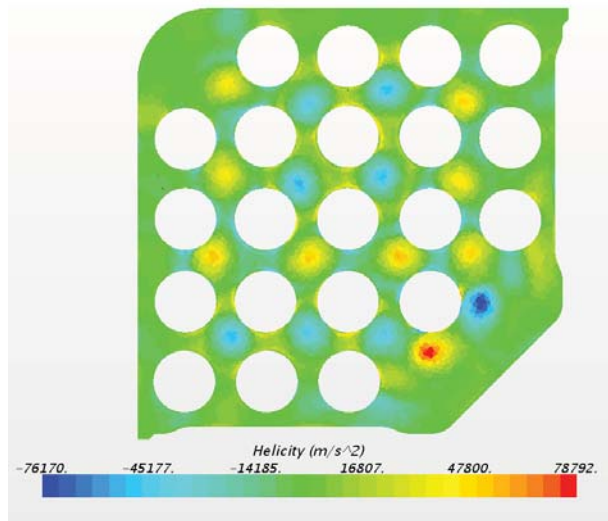


Figure 7. Helicity in a plane 0.06 m above the spacer grid

Figure 8 shows droplets colored with the same index at the inlet and at the outlet, i.e. particles colored yellow at the inlet will continue to have that color throughout the domain. Note that the lower left corner on the inlet view corresponds to the upper right corner of the outlet view as the inlet view is seen from below while the outlet is seen from above. It can be observed that particles originally released in one lateral position of the domain will most likely not travel far in the horizontal direction. Note that this observation is specific to the assumed adiabatic conditions and is likely to be affected by crossflows driven by non-uniform radial power distribution.

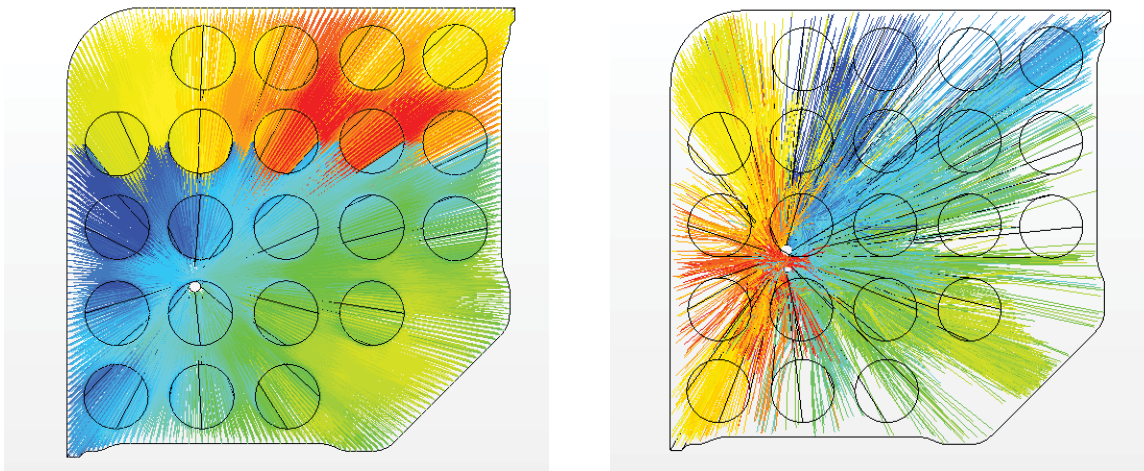
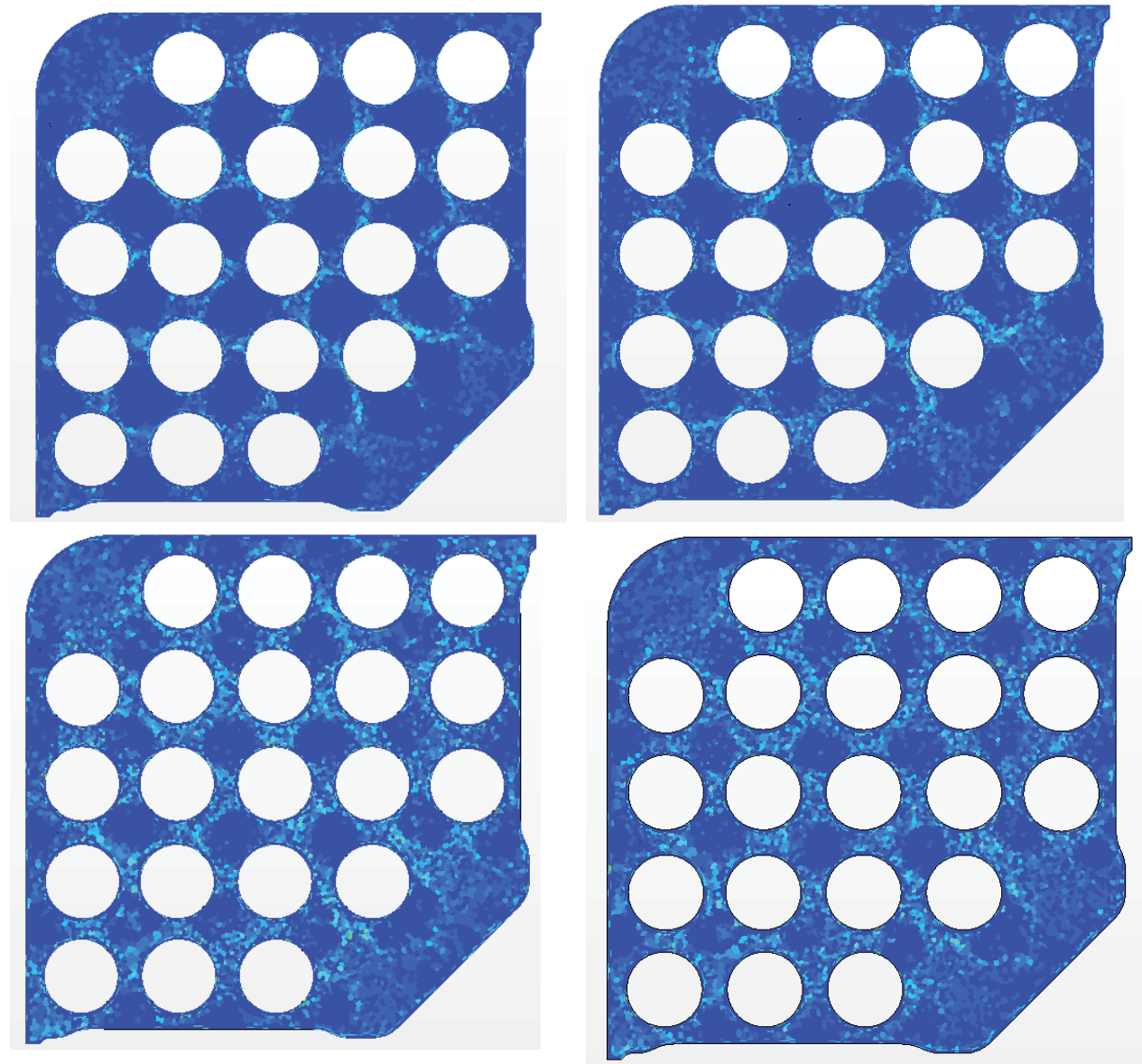


Figure 8. Colored droplets at the inlet (left) and at the outlet (right)

### 3.3. Droplet Distribution

The droplet distribution in a cross-sectional plane 0.02 m downstream the top of the spacer grid is shown in Figure 9 for four different droplet diameters; 50, 100, 200 and 300  $\mu\text{m}$ . It is observed that the droplet distribution becomes more even for larger droplet diameters, i.e. larger Stokes numbers. For droplets with a diameter of 50  $\mu\text{m}$ , most of the droplets accumulate outside the center of each subchannel. When comparing with Figure 10, where a projected velocity field is shown in the same cross-sectional plane, it

is seen that the areas with almost no droplets correlate with areas with large vortices (Figure 7 and Figure 9). For the larger droplet diameters this correlation decreases. These results confirm the reasoning in section 3.1 that droplets with larger Stokes numbers do not adjust as much to the flow field, i.e. they have (as expected) a more ballistic behavior.



**Figure 9. Droplet distribution (white regions have more droplets and blue regions have less droplets) in a cross-sectional plane downstream the spacer grid for  $D_p=50 \mu\text{m}$  (top left),  $D_p=100 \mu\text{m}$  (top right),  $D_p=200 \mu\text{m}$  (lower left) and  $D_p=300 \mu\text{m}$  (lower right)**

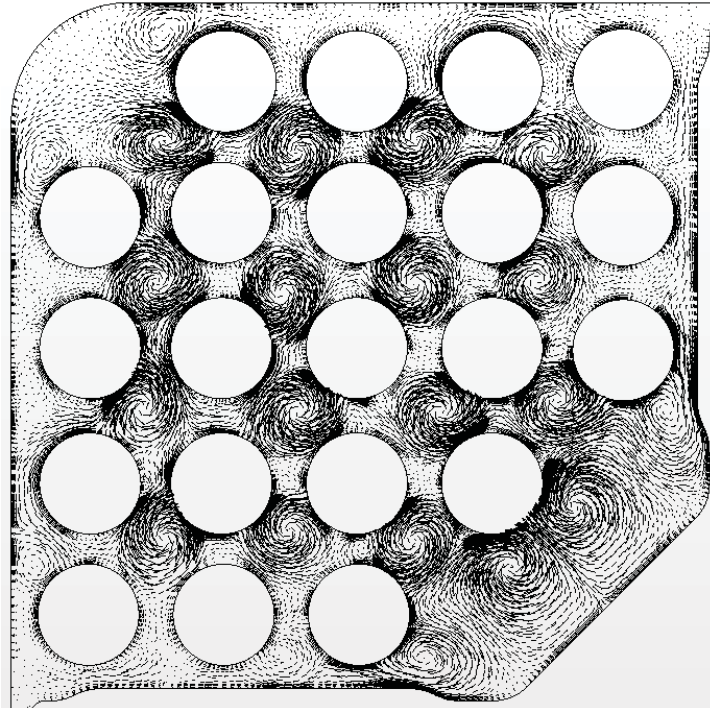


**Figure 10. Velocity vector field projected in a cross-sectional plane 0.02 m downstream the spacer grid**

#### 4. CONCLUSIONS AND OUTLOOK

An Euler-Lagrangian CFD model of a 5x5 Westinghouse Optima3 quarter bundle fuel assembly was used in order to investigate the effect of the spacer grid on the droplet deposition. Different droplet diameters were considered and it was generally found that particles with small diameters (small Stokes numbers) tend to deposit less due to a smaller response time, i.e. the smaller droplets will respond quicker to changes in the flow. The droplet distribution in a cross-sectional plane was also studied and a correlation between a small particle volume fraction and a strong vorticity, that increased with decreasing droplet diameter, was found.

In the present study a simplified isothermal model was used. In future studies, it would be beneficial to also include the energy equation in order to see how heat transfer affects the flow field and the droplet deposition. An escape boundary conditions was set for the droplets on the rod walls. Adding a film model at these walls, including entrainment of droplets from the film to the steam flow, would be more physical and could be included in the models. The measured drop size distributions from [8] will also be considered in the future. In addition, the coupling between CFD calculations over a single grid span and realistic subchannel simulations of the entire fuel bundle will be further developed, using the two-phase three-field analysis code MEFISTO [9].

#### NOMENCLATURE

BWR	Boiling Water Reactor
CFD	Computational Fluid Dynamics
$D_H$	Hydraulic diameter of a subchannel
$D_p$	Particle diameter

PWR	Pressurized Water Reactor
St	Stokes Number
U	Mean velocity
$\tau_g$	Characteristic time scale of the flow
$\tau_p$	Droplet response time
$\mu_g$	Dynamic viscosity

## REFERENCES

1. D. Y. Sheng, J.-M. Le Corre and S. Andersson, “CFD investigation of drop deposition enhancement downstream mixing van grids near BWR dryout conditions”, *Proceedings of the 15<sup>th</sup> International Topical Meeting on Nuclear Reactor Thermal – Hydraulics, NURETH-15*, Pisa, Italy, May 12-17, NURETH15-421 (2013)
2. M. Damsohn, *Liquid films and droplet deposition in a BWR fuel element*, PhD Thesis, DISS. ETH No. 19527, Zurich (2011)
3. K. Goodheart, A. Ylönen, V. De Cacqueray and H.-M. Prasser, “CFD validation of void distribution in a rod bundle with spacer”, *Proceedings of the 2014 22<sup>nd</sup> International Conference on Nuclear Engineering, ICONE22*, Prague, Czech Republic, July 7-11, ICONE22-30741 (2014)
4. S. Mimouni, F. Archambeau, M. Boucker, J. Lavieville and C. Morel, “A second order turbulence model based on a Reynolds stress approach for two-phase boiling flow and application to fuel assembly analysis”, *Nuclear Eng. and Design* **240**, pp. 2225-2232 (2010)
5. M.V. Holloway, D.E. Beasley and M.E. Conner , “Investigation of swirling flow in rod bundle subchannels using computational fluid dynamics”, *Proceedings of International Conference on Nuclear Engineering 2006, ICONE14*, Miami, Florida. USA, July 17-20 2006, ICONE14-89068
6. S. Elghobashi, “On predicting particle-laden turbulent flows”, *Applied Scientific Research*, **52**, pp. 229-237 (1994)
7. C. Crowe, M. Sommerfeld and Y. Tsuji, *Multiphase flows with droplets and particles*, CRC Press (1998)
8. J.-M. Le Corre, U. C. Bergmann, A. Hallehn, H. Tejne, F. Waldemarsson, B. Morenius and R. Baghai, “Detailed measurements of local parameters in annular two-phase flow in fuel bundle under BWR operating conditions,” *Proceedings of the 16<sup>th</sup> International Topical Meeting on Nuclear Reactor Thermal – Hydraulics, NURETH-16*, Chicago, USA, Aug. 30- Sept. 4, NURETH16-13530 (2013)
9. C. Adamsson and J.-M. Le Corre, “Modeling and validation of a mechanistic tool (MEFISTO) for the prediction of critical power in BWR fuel assemblies,” *Nucl. Eng. and Design*, **241**, pp. 2843-2858 (2011)